IEEE Access
Multidisciplinary ⋮ Rapid Review ⋮ Open Access Journal

Received 25 September 2023, accepted 28 October 2023, date of publication 6 November 2023, date of current version 13 November 2023.

*Digital Object Identifier 10.1109/ACCESS.2023.3330586*

RESEARCH ARTICLE

# Uncertain Systems Motion Synchronization

**ŠEJLA DŽAKMIĆ[1], AMEL RAMDEDOVIĆ[1], AND ASIF ŠABANOVIĆ[1,2], (Life Senior Member, IEEE)**
[1]Department of Electrical Engineering, International University of Sarajevo, 71000 Sarajevo, Bosnia and Herzegovina
[2]Academy of Sciences and Arts of Bosnia and Herzegovina, 71000 Sarajevo, Bosnia and Herzegovina

Corresponding author: Šejla Džakmić (sdzakmic@ius.edu.ba)

This work was supported in part by the Ministry of Science, Higher Education and Youth, Sarajevo, Bosnia and Herzegovina, under Grant 27-02-35-3517-22/22.

**ABSTRACT** In the operation of large-scale manufacturing equipment, accurate tracking of the desired trajectory and overall motion synchronizations are the keys to ensuring the products' high quality. These multi-axis plants are highly coupled nonlinear systems with a range of uncertainties (parametric uncertainties, unmodelled dynamics, cross-coupling between axes, and external disturbances). That makes the control design for such systems a challenging task. In this paper, a Lyapunov-based design for motion tracking and/or cross-coupling synchronization control for multi-axis systems is proposed. The aim is to develop a general framework for the design of motion tracking and/or cross-coupling synchronization. The proposed design is based on a specific structure of the generalized control error and design of control which enforces a predefined form of the Lyapunov function time derivative. The structure of the generalized error allows the application of the same controller design procedure for motion tracking and/or cross-coupled synchronization control in either configuration or operation space. In the proposed design compensation of uncertainties and the convergence of the generalized error are treated separately. The compensation for the uncertainties is realized by the application of an unknown input observer within the controller structure. That yields efficient compensation of the projection of the system uncertainties to the generalized error. In ensuring the desired convergence and stability the Lyapunov function time derivative is used as a design parameter. It could be selected so that closed-loop dynamics exhibits asymptotic or finite-time convergence. The proposed design results in a simple easy-to-implement controller structure with a small number of design parameters. The details of the design procedure and the proposed controller are evaluated in simulation and experiments for a coupled 4-axis system.

**INDEX TERMS** Motion control, motion synchronization, cross-coupling control, sliding mode, robust control, disturbance observer.

## I. INTRODUCTION

Modern industrial equipment is highly coupled nonlinear systems with a range of uncertainties (parametric uncertainties, unmodelled dynamics, cross-coupling between axes, external disturbances), which makes a control design for such plants a challenging task. The operation of such complex multi-axis systems or systems realized by multiple motors driving a single load with high inertia in addition to standard motion tracking loops requires a cross-coupling control to realize synchronization requirements. Specific problems appear in the system with time delay which acts as disturbances to the cross-coupling control. In current literature, a variety of solutions addressing the cross-coupling synchronization problem are presented. Most of these are developed as an addition to the control design for specific machine or axis configurations.

The Lyapunov approach for synchronization of a two-slider system is discussed in [1] with a nonlinear force coupling model as a basis for the control design. The robust synchronization controller is discussed in [2]. Here the cross-coupling error is defined as a difference in the position error of each axis and its two adjacent axes. Such selection makes the cross-coupling synchronization matrix

The associate editor coordinating the review of this manuscript and approving it for publication was Wonhee Kim.

singular and imposes restrictions on the controller parameter. A system with a centralized motion tracking controller and a decoupling synchronization controller for each axis is discussed in [3]. The decoupling controllers are designed based on mean deviation while unmeasurable states and nonlinearities are managed by a neural network. A cross-coupling structure applicable for the accurate contouring control is discussed in [4]. In [5] a continuous sliding mode controller is applied for synchronization of the dual spindle system. The tracking error is augmented by the synchronization error and the sliding mode controller is designed for the augmented system. A hierarchical sliding mode control discussed in [6] for a multi-axis hydraulic servo-drive system consists of an adaptive backstepping tracking controller, a neural network synchronization controller, and a higher-order sliding mode controller working in parallel. In [7] an adaptive motion control based on position averaging and decentralized adaptive controllers for each axis is proposed for synchronization of the multi-axis system. In [8] synchronization based on cross-coupled control is applied to a 2-axis gantry system. The solution is based on a combination of the tracking and synchronization errors and the cascade controller. It is claimed that the control design does not require information on the detailed plant model. In [9] a robust synchronization control with the possibility to use position, velocity, or acceleration as a synchronization error and $H_\infty$ controller is discussed. The key idea is to shape the position reference by a prefilter in each axis combined with $H_\infty$ a mixed sensitivity method. The application of a fuzzy PID controller for synchronization of a multi-axis system is discussed in [10] and applied to a hydraulic dual-axe system. The synchronization of a 3-dof planar parallel robotic manipulator with uncertain dynamics using terminal sliding mode is shown and simulation results are presented in [11]. The effects of chattering are suppressed by the introduction of the synchronization integral action in the system. Teleoperation as a specific arrangement that requires synchronization of motion and implemented forces is discussed in some works. The synchronized bilateral teleoperation system with predefined-time convergence is discussed in [12] and [13] the Q-learning algorithm is applied for the synchronized teleoperated system with cognitive guiding force. In [14] independent adaptive-fuzzy compensation of friction is applied for each axis and a sliding mode synchronization controller is proposed. The control input has a feed-forward term and a discontinuous term that may cause chattering. The proposed synchronization error matrix is singular, and the synchronization error gain should be carefully selected. Recent work in the synchronization of networked control systems [15] discusses the compensation of the uncertainties induced by network and cooperative distributed model predictive control strategy. The discrete-time synchronization control of a dual-motor networked manipulator is discussed in [16]. The main contribution is the explicit consideration of sampled data coupling and transmission delays among coordinated manipulators. In [17] an application to networked manipulators tracking trajectories in operation space is discussed. The discrete-time sliding mode is applied combined with distributed operation-space tracking control to guarantee stability and dynamic performance. The cross-coupling control of dual motors in the networked control framework is discussed in [18]. The feasibility and stability of the proposed cross-coupling control system are verified theoretically.

As shown above, several robust and adaptive control strategies dealing with the problem of motion synchronization are reported in the literature. Along with the application of the different control frameworks, the problem of the formulation of the cross-coupling error is one of the issues that attracts attention. Cross-coupling is perceived as a supporting mechanism tightly dependent on the structure of the system under control and the cross-coupling is studied for the structure of the system under analysis. The work in which a general solution is discussed often has a specific structure of the cross-coupling error. All of this shows that the search for a solution that would have a straightforward design procedure, fever design parameters, and could be applied for various problems in motion control is still an open problem.

In this paper, a Lyapunov-based design framework for motion tracking with or without cross-coupling synchronization control in multi-axis systems is proposed. The proposed design is based on the formulation of a generalized control error as a linear or nonlinear combination of the position tracking or synchronization error and its derivative. Such a selection of the generalized error yields a relative order one of the generalized error dynamics. That provides a basis for the application of the same procedure in controller design for motion tracking and/or cross-coupling synchronization in either configuration or operation space. The Lyapunov function is selected as a quadratic form of the generalized error. Its time derivative is used as a design parameter allowing selection that would yield asymptotic or finite-time convergence of the generalized error. In the design, the compensation of uncertainties and the convergence of the generalized error are treated separately. The application of an unknown input observer within the controller structure yields efficient compensation of the projection of the system uncertainties to the generalized error. A separate term of the control input that enforces the specified Lyapunov function derivative thus ensures the convergence and stability of the closed-loop system. This term enforces the desired general error convergence as well. It is shown that such a design procedure could be applied to wide-range motion tracking problems with or without cross-coupling synchronization. The different problems could be implemented by coupling control errors or by coupling the control outputs. The former solution is applicable for systems requiring redundancy if some axis controllers have failed. The main contribution of this work is in proposing a general framework that allows consistent design of motion control systems that results in a simple easy-to-implement controller with a small number

of well-defined design parameters. The details of the design procedure and the proposed controller are evaluated in simulation and experiments for a coupled 4-axis system.

The rest of the paper is organized as follows. In Section II the dynamics of the system, the compensation of uncertainties, and the dynamics of the motion tracking, synchronization, and coupled motion tracking and synchronization errors are formulated. In Section III Lyapunov-based control system design is discussed and the structure of the control input for systems with asymptotic and finite time convergence (sliding mode motion) are derived. In Section IV the effectiveness of the proposed algorithm is confirmed by presenting the simulation and experimental results.

## II. PROBLEM STATEMENT

In this section, the system dynamics and compensation of uncertainties along with dynamics of the control errors for motion tracking, synchronization, and coupled error are derived and formulated in a way that would allow consistent control design.

### A. PLANT DESCRIPTION

A general motion system of $n$- actuators with uncertain dynamics is considered. The configuration space dynamics is given by

$$\mathbf{A}(\mathbf{q})\ddot{\mathbf{q}} + \mathbf{b}(\mathbf{q},\dot{\mathbf{q}}) + \mathbf{g}(\mathbf{q}) + \boldsymbol{\tau}_{ext} = \boldsymbol{\tau} \tag{1}$$

Here $\mathbf{q}^T = \begin{bmatrix} q_1 \ \dots \ q_n \end{bmatrix}$ stands for the actuators position vector; $\mathbf{A}(\mathbf{q})$ is a positive definite system inertia matrix; $\boldsymbol{\tau}^T = \begin{bmatrix} \tau_1 \ \dots \ \tau_n \end{bmatrix}$ stands for the input control vector; $\mathbf{b}^T(\mathbf{q},\dot{\mathbf{q}}) = \begin{bmatrix} b_1 \ .. \ b_n \end{bmatrix}$ stands for the vector of Coriolis and centripetal forces;$\mathbf{g}^T(\mathbf{q}) = \begin{bmatrix} g_1 \ .. \ g_n \end{bmatrix}$ stands for the vector of gravitational forces;$\boldsymbol{\tau}_{ext}^T = \begin{bmatrix} \tau_1^{ext} \ \dots \ \tau_n^{ext} \end{bmatrix}$ is the vector of external forces acting on actuators. The vectors $\boldsymbol{\tau}, \mathbf{b}(\mathbf{q},\dot{\mathbf{q}})\,\mathbf{g}(\mathbf{q}), \boldsymbol{\tau}_{ext}$ and their components $\tau_k\ b_k(\mathbf{q},\dot{\mathbf{q}})$, $g_k(\mathbf{q})$, $\tau_k^{ext}$, $k = 1, 2, \dots, n$ are assumed bounded by known upper and lower bounds consistent with the operation domain $(\mathbf{q},\dot{\mathbf{q}}) \in D$ of the system. The inertia matrix has bounded elements $a_{ij}(\mathbf{q})$, $1 \le i, j \le n$, hence matrix $\mathbf{A}(\mathbf{q})$ is bounded by known lower and upper bounds. This matrix can be expressed as a sum of its nominal value and uncertainties $\mathbf{A}(\mathbf{q}) = A_n + \Delta\mathbf{A}(\mathbf{q})$. The $\mathbf{A}_n$ is assumed known. The $\Delta\mathbf{A}(\mathbf{q})$ stands for bounded inertia matrix uncertainties. If dynamics (1) stands for the description of $n-$ individual axes, then $\mathbf{A}(\mathbf{q})$ as well as $\mathbf{A}_n$ are positive definite diagonal matrices. The dynamics of the system (1) could be written in the following form

$$\begin{cases} \mathbf{A}_n\ddot{\mathbf{q}} = \boldsymbol{\tau} - \boldsymbol{\tau}^{dis} \\ \boldsymbol{\tau}^{dis} = \mathbf{b}(\mathbf{q},\dot{\mathbf{q}}) + \mathbf{g}(\mathbf{q}) + \boldsymbol{\tau}_{ext} + \Delta\mathbf{A}\ddot{\mathbf{q}} \end{cases} \tag{2}$$

Here $\boldsymbol{\tau}^{disT} = \begin{bmatrix} \tau_1^{dis} \ .. \ \tau_n^{di} \end{bmatrix}$ stands for the system's bounded generalized disturbance. In (2) the disturbances are decoupled but the coupling due to the inertia matrix $\mathbf{A}(\mathbf{q})$ may remain if the nominal matrix $\mathbf{A}_n$ is not diagonal.

Let pair $(\dot{\mathbf{q}} = \boldsymbol{\omega}, \boldsymbol{\tau})$ is measured, the dynamics of the generalized disturbance is assumed as $\dot{\tau}^{dis} = \mathbf{0}$ and an auxiliary variable is defined as $\boldsymbol{\xi} = \boldsymbol{\tau}^{dis} + \mathbf{L}_q\mathbf{A}_n\boldsymbol{\omega}$. As shown in [19] and [20] an observer estimating generalized disturbance $\boldsymbol{\tau}^{dis}$ could be expressed as

$$\begin{cases} \dot{\hat{\boldsymbol{\xi}}} = -\mathbf{L}_q\hat{\boldsymbol{\xi}} + \mathbf{L}_q\left(\boldsymbol{\tau} + \mathbf{L}_q\mathbf{A}_n\boldsymbol{\omega}\right) \\ \hat{\boldsymbol{\tau}}^{dis} = \hat{\boldsymbol{\xi}} - \mathbf{L}_q\mathbf{A}_n\boldsymbol{\omega};\ \mathbf{L}_q > 0; \\ \dot{\hat{\boldsymbol{\tau}}}^{dis} + \mathbf{L}_q\hat{\boldsymbol{\tau}}^{dis} = \mathbf{L}_q\boldsymbol{\tau}^{dis} \end{cases} \tag{3}$$

The observer (3) yields the dynamics of the estimated generalized disturbance as $\dot{\hat{\boldsymbol{\tau}}}^{dis} + L_q\dot{\hat{\boldsymbol{\tau}}}^{dis} = \mathbf{L}_q\boldsymbol{\tau}^{dis}$. Here matrix $\mathbf{L}_q > 0$ is the design parameter. The more complex observer could be designed [20], [21], [24] but (3) usually works well in motion control systems.

Insertion of the system input $\boldsymbol{\tau} = \boldsymbol{\tau}^{con} + \hat{\boldsymbol{\tau}}^{dis}$ into (2) yields the dynamics of system with disturbance observer as

$$\boldsymbol{\tau} = \boldsymbol{\tau}^{con} + \hat{\boldsymbol{\tau}}^{dis} \Rightarrow \begin{cases} \mathbf{A}_n\ddot{\mathbf{q}} = \boldsymbol{\tau}^{con} - \mathbf{p}\left(\hat{\boldsymbol{\tau}}^{dis}\right) \\ \hat{\boldsymbol{\tau}}^{dis} + \mathbf{L}\hat{\boldsymbol{\tau}}^{dis} = \mathbf{L}\boldsymbol{\tau}^{dis};\ \mathbf{L} > 0 \\ \mathbf{p}\left(\hat{\boldsymbol{\tau}}^{dis}\right) = \left(\boldsymbol{\tau}^{dis} - \hat{\boldsymbol{\tau}}^{dis}\right) \underset{t\to\infty}{\to} 0 \end{cases}$$
$$\boldsymbol{\tau}_q^{con} = \begin{bmatrix} \tau_1^{con} & \dots & \tau_n^{con} \end{bmatrix}^T;\ \boldsymbol{\tau}^{dis} = \begin{bmatrix} \tau_1^{dis} & \dots & \tau_n^{dis} \end{bmatrix}^T \tag{4}$$

Here the $\boldsymbol{\tau}^{con}$ stands for the control input generated by the control system; $\mathbf{p}\left(\hat{\boldsymbol{\tau}}^{\text{dis}}\right)$ stands for generalized disturbance estimation error with bounded components $p_k = \tau_k^{dis} - \hat{\tau}_k^{dis}$, $k = 1, \dots, n$. The compensated system (4) stands for the $n-$ double integrators with known inertia and $n$- order dynamics of the estimation error. Selection of the design parameter $\mathbf{L}_q > 0$ guarantees convergence of the estimation error $\mathbf{p}\left(\hat{\boldsymbol{\tau}}^{\text{dis}}\right)^q$ and should be selected such that the separation of dynamics of the observer and closed loop system is satisfied. The dynamics (4) is similar to the system dynamics (2). This similarity points out that the estimation error $\mathbf{p}\left(\hat{\boldsymbol{\tau}}^{\text{dis}}\right)$ could be treated as an uncompensated disturbance and should be considered in the design of the closed-loop controller [19]. This way the compensation of the uncertainties in the system will be realized in part by the estimation of generalized disturbance and in part by the selection of the closed-loop control.

If the nominal inertia matrix $\mathbf{A}_n$ and observer gain matrix $\mathbf{L}_q$ are diagonal with elements $a_{nkk} \neq 0$ and $l_k > 0, k = 1, .., n$ respectively the components of the observer (3) could be written as

$$\begin{cases} \dot{\hat{\xi}} = -l_k\hat{\xi}_k + l_k\left(\tau_k + l_k a_{nkk}\omega_k\right), \\ \hat{\tau}_k^{dis} = \hat{\xi}_k - l_k a_{nkk}\omega_k;\ l_k > 0;\ k = 1, \dots, n \\ \dot{\hat{\tau}}_k^{dis} + l_k\hat{\tau}_k^{dis} = l_k\tau_k^{dis} \end{cases} \tag{5}$$

Expressing the components of the control input as $\tau_k = \tau_k^{con} + \hat{\tau}_k^{\text{dis}}$ the dynamics of the actuators could be described as

$$\begin{cases} \dot{q}_k = \omega_k; \quad k = 1, 2, \dots, n \\ a_{nkk}\dot{\omega}_k = \tau_k^{con} - p_k\left(\hat{\tau}_k^{dis}\right) \\ p_k\left(\hat{\tau}_k^{dis}\right) = \tau_k^{dis} - \hat{\tau}_k^{dis} \end{cases} \tag{6}$$

The dynamics (2) or (4) could be used as a starting point in the motion control design. The difference is just in the structure of the system's uncertainties $\boldsymbol{\tau}^{\text{dis}}$ (in (2)) and $\mathbf{p}\left(\hat{\boldsymbol{\tau}}^{dis}\right)$ (in (4)). That allows the application of the same design for both descriptions.

### B. THE MOTION AND TASK ERROR DYNAMICS

In multi-axis systems with independent axis controllers, the desired relationship is kept by the selection of the configuration space references based on the system task.

By assumption, from the task description, the unique reference $\mathbf{q}^{\text{ref}} \in \Re^{n\times 1}$ with elements $q_k^{\text{ref}}, k = 1, \ldots, n$ could be determined. The dynamics of the tracking error $\mathbf{e}_q^T = \left[\, e_{q1} \;..\; e_{qn} \,\right], e_{qk} = q_k - q_k^{\text{ref}}$ for the system dynamics (2) and (4) could be expressed as

$$\begin{cases} \mathbf{e}_q = \mathbf{q} - \mathbf{q}^{\text{ref}} \\ \ddot{\mathbf{e}}_q = \boldsymbol{\tau}_q - \boldsymbol{\tau}_q^{\text{dis}} \end{cases}$$
$$\begin{cases} \boldsymbol{\tau}_q = \begin{cases} \mathbf{A}_n^{-1}\boldsymbol{\tau} & \text{for dynamics (2)} \\ \mathbf{A}_n^{-1}\boldsymbol{\tau}^{\text{con}} & \text{for dynamics (4)} \end{cases} \\ \boldsymbol{\tau}_q^{\text{dis}} = \begin{cases} \mathbf{A}_n^{-1}\boldsymbol{\tau}^{\text{dis}} + \ddot{\mathbf{q}}^{\text{ref}} & \text{for dynamics (2)} \\ \mathbf{A}_n^{-1}\mathbf{p}\left(\hat{\boldsymbol{\tau}}^{\text{dis}}\right) + \ddot{\mathbf{q}}^{\text{ref}} & \text{for dynamics (4)} \end{cases} \end{cases} \tag{7}$$

The coupling between axes is defined by the system structure and the task specification. In such system arrangements, possible deviations in the individual axis are not "shared" with other control loops directly but are reflected to the other axes via system-coupled dynamics.

Another way to execute the desired task is by designing the control directly in the operation space. Let the operation task for a system be defined by $\mathbf{h}(\mathbf{q}) = \mathbf{h}^{\text{ref}}$. Here $\mathbf{h}(\mathbf{q})$ could be a linear or nonlinear continuous function. The dynamics of the task error $\mathbf{e}_h$ for the system dynamics (2) and (4) could be expressed as

$$\begin{cases} \mathbf{e}_h = \mathbf{h}(\mathbf{q}) - \mathbf{h}^{\text{ref}} \\ \ddot{\mathbf{e}}_h = \mathbf{f}_h - \mathbf{f}_h^{\text{dis}} \end{cases}$$
$$\begin{cases} \mathbf{f}_h = \begin{cases} \mathbf{J}\mathbf{A}_n^{-1}\boldsymbol{\tau} & \text{for dynamics (2)} \\ \mathbf{J}\mathbf{A}_n^{-1}\boldsymbol{\tau}^{\text{con}} & \text{for dynamics (4)} \end{cases}; \\ \qquad\qquad \mathbf{J} = \dfrac{\partial \mathbf{h}(\mathbf{q})}{\partial \mathbf{q}} \in \Re^{n\times n} \\ \mathbf{f}_h^{\text{dis}} = \begin{cases} \mathbf{J}\mathbf{A}_n^{-1}\boldsymbol{\tau}^{\text{dis}} - \dot{\mathbf{J}}\dot{\mathbf{q}} + \ddot{\mathbf{h}}^{\text{ref}} & \\ \qquad\qquad \text{for dynamics (2)} & \\ \mathbf{J}\mathbf{A}_n^{-1}\mathbf{p}\left(\hat{\boldsymbol{\tau}}^{\text{dis}}\right) - \dot{\mathbf{J}}\dot{\mathbf{q}} + \ddot{\mathbf{h}}^{\text{ref}} & \\ \qquad\qquad \text{for dynamics (4)} & \end{cases} \end{cases} \tag{8}$$

Here $\mathbf{J} \in \Re^{n\times n}$ is assumed full-rank matrix with bounded elements in the operational domain of the system; $\mathbf{f}_h$ stands for the control input and $\mathbf{f}_h^{\text{dis}}$ stands for the disturbance. In (8) the cross-coupling is realized due to the formulation of the task $\mathbf{h}(\mathbf{q})$ but, similarly, as in the independent axes control, there is no cross-coupling on the error level. Note that the task could also be formulated as $\mathbf{h}(\mathbf{q}) = \mathbf{T}_h\mathbf{q} = \mathbf{h}^{\text{ref}}$, where $\mathbf{T}_h \in \Re^{n\times n}$ is assumed constant full rank matrix. Then dynamics (8) holds with $\mathbf{J} = \mathbf{T}_h \in \Re^{n\times n}$ task tracking error $\mathbf{e}_h = \mathbf{T}_h\mathbf{q} - \mathbf{h}^{\text{ref}}$.

The dynamics (5) and (8) have the same form and usage of the dynamics (2) or (4) is reflected in the structure of the control input and disturbance in the error space. Further in the paper only expressions for dynamics (2) will be given. The derivations for dynamics (4) are straightforward by changing the control input $\boldsymbol{\tau}$ by $\boldsymbol{\tau}^{con}$ and the disturbance $\boldsymbol{\tau}^{\text{dis}}$ by the error in disturbance estimation $\mathbf{p}\left(\hat{\boldsymbol{\tau}}^{\text{dis}}\right)$.

### C. THE SYNCHRONIZATION ERROR DYNAMICS

For a system with configuration or operation space control the synchronization task could be interpreted as the addition to the motion tracking with cross-coupling realized in such a way that control errors converge to zero synchronously. The cross-coupling error could be defined in both the configuration and the operation space. Let $\mathbf{e}_{sq} = \mathbf{T}_{sq}\mathbf{e}_q$ stands for the cross-coupling error in the configuration space and, $\mathbf{e}_{sh} = \mathbf{T}_{sh}\mathbf{e}_h$ stands for the task cross-coupling error in the operation space. Matrices $\mathbf{T}_{sq} \in \Re^{n\times n}$ and $\mathbf{T}_{sh} \in \Re^{n\times n}$ are assumed regular. If cross-coupling relationships $\mathbf{e}_{sq} = 0$ or $\mathbf{e}_{sh} = 0$ are enforced by control then, due to the structure of the cross-coupling matrices $\mathbf{T}_{sq}$ and $\mathbf{T}_{sh}$ the $\mathbf{e}_q = 0$ and/or $\mathbf{e}_h = 0$ will be enforced as well. This shows that synchronization and motion tracking or task tracking could be enforced concurrently. If the synchronization and the motion or task tracking are applied together then the system may exhibit a certain level of redundancy.

The dynamics of the cross-coupling error in configuration space could be expressed as

$$\begin{cases} \mathbf{e}_{sq} = \mathbf{T}_{sq}\mathbf{e}_q \\ \ddot{\mathbf{e}}_{sq} = \mathbf{f}_{sq} - \mathbf{f}_{sq}^{dis} \end{cases}$$
$$\begin{cases} \mathbf{f}_{sq} = \mathbf{T}_{sq}\mathbf{A}_n^{-1}\boldsymbol{\tau} \\ \mathbf{f}_{sq}^{dis} = \mathbf{T}_{sq}\left(\mathbf{A}_n^{-1}\boldsymbol{\tau}^{dis} + \ddot{\mathbf{q}}^{ref}\right) \end{cases} \tag{9}$$

where $\mathbf{f}_{sq}$ and $\mathbf{f}_{sq}^{dis}$ stand for the synchronization control and disturbance inputs, respectively.

The dynamics of the cross-coupling error in operation space $\mathbf{e}_{sh}$ with task $\mathbf{h}(\mathbf{q}) = \mathbf{T}_h\mathbf{q} = \mathbf{h}^{ref}$ and cross-coupling defined by $\mathbf{e}_{sh} = \mathbf{T}_{sh}\mathbf{e}_h$ could be determined as

$$\begin{cases} \mathbf{e}_{sh} = \mathbf{T}_{sh}\mathbf{e}_h \\ \ddot{\mathbf{e}}_{sh} = \mathbf{f}_{sh} - \mathbf{f}_{sh}^{dis} \end{cases}$$
$$\begin{cases} \mathbf{f}_{sh} = \mathbf{T}_{sh}\mathbf{J}\mathbf{A}_n^{-1}\boldsymbol{\tau} \\ \mathbf{f}_{sh}^{dis} = \mathbf{T}_{sh}\left(\mathbf{J}\mathbf{A}_n^{-1}\boldsymbol{\tau}^{dis} - \dot{\mathbf{J}}\dot{\mathbf{q}} + \ddot{\mathbf{h}}^{ref}\right) \end{cases} \tag{10}$$

where $\mathbf{f}_{sh}$ and $\mathbf{f}_{sh}^{dis}$ stand for the synchronization control and disturbance inputs, respectively.

The dynamics (7), (8), (9) and (10) point out to the possibility to formulate the synchronization of the motion control of multiple axes in a few ways:

i. formulation of synchronization control as a task control in operation space with the task error $\mathbf{e}_{sh} = \mathbf{T}_h\mathbf{q} - \mathbf{h}^{ref}$ expressed as in (8) with $\mathbf{J} = \mathbf{T}_h \in \Re^{n\times n}$. In this case, cross-coupling of system motion is realized by a choice of matrix $\mathbf{T}_h \in \Re^{n\times n}$;
ii. the configuration space design based on the usage of the motion tracking error $\mathbf{e}_q$ and the cross-coupling error $\mathbf{e}_{sq} = \mathbf{T}_{sq}\mathbf{e}_q$. The realization could be implemented: (a) by establishing the coupled configuration space control error $\mathbf{e}_{qsq}(\mathbf{e}_q, \mathbf{e}_{sq})$ or (b) by merging control inputs obtained from the motion controller $\boldsymbol{\tau}_q$ and the control input $\mathbf{f}_{sq}$ obtained from the cross-coupling synchronization controller to form coupled control input $\mathbf{f}_{qsq}\left(\boldsymbol{\tau}_q, \mathbf{f}_{sq}\right)$;
iii. the operation space design based on the usage of the task error $\mathbf{e}_h$ and cross-coupling error $\mathbf{e}_{sh} = \mathbf{T}_{sh}\mathbf{e}_h$. The realization could be implemented, similarly as in configuration space, (a) by establishing the coupled configuration space control error $\mathbf{e}_{hsh}(\mathbf{e}_h, \mathbf{e}_{sh})$ or (b) by merging the control inputs obtained from the task controller $\mathbf{f}_h$ and the control input $\mathbf{f}_{sh}$ obtained from the cross-coupling synchronization controller to form coupled operation space control input $\mathbf{f}_{hsh}(\mathbf{f}_h, \mathbf{f}_{sh})$.

In both configuration and operation spaces, a certain level of redundancy could be obtained if the motion and the cross-coupling are merged at the control input level.

### D. THE COUPLED ERROR DYNAMICS

Before discussing the control design let us closely examine the dynamics of the coupled errors in configuration space $\mathbf{e}_{qsq}(\mathbf{e}_q, \mathbf{e}_{sq})$ and operation space $\mathbf{e}_{hsh}(\mathbf{e}_h, \mathbf{e}_{sh})$ defined as in (11) and (12) respectively.

$$\left(\mathbf{e}_q \& \mathbf{e}_{sq}\right) \Rightarrow \begin{cases} \mathbf{e}_{qsq} = \mathbf{e}_q + \alpha\mathbf{S}_q\mathbf{e}_{sq} = \Omega_{qs}\mathbf{e}_q \\ \Omega_{qsq} = \mathbf{I} + \alpha\mathbf{S}_q\mathbf{T}_{sq};\ \alpha > 0 \end{cases} \tag{11}$$

$$(\mathbf{e}_h \& \mathbf{e}_{sh}) \Rightarrow \begin{cases} \mathbf{e}_{hsh} = \mathbf{e}_h + \beta\mathbf{S}_h\mathbf{e}_{sh} = \Omega_{hs}\mathbf{e}_h \\ \Omega_{hsh} = \mathbf{I} + \beta\mathbf{S}_h\mathbf{T}_{sh};\ \beta > 0 \end{cases} \tag{12}$$

Here gains $\alpha > 0$ and $\beta > 0$ stand for the weight of the cross-coupling synchronization error and could be scalars or diagonal $n \times n$ matrices. Matrices $S_q\left(\mathbf{T}_{sq}\right)$ and $S_h\left(\mathbf{T}_{sh}\right)$ are diagonal with elements $s_{qkk}\left(\mathbf{T}_{sq}\right)$ and $s_{hkk}\left(\mathbf{T}_{sh}\right)$ equal to the sign of the corresponding diagonal elements of the matrices $\mathbf{T}_{sq}$ and $\mathbf{T}_{sh}$ respectively. The transformation matrices $\boldsymbol{\Omega}_{qsq}$ and $\boldsymbol{\Omega}_{hsh}$ are regular by construction.

The dynamics of the coupled error in configuration space $\mathbf{e}_{qsq}(\mathbf{e}_q, \mathbf{e}_{sq})$ could be expressed as

$$\begin{cases} \mathbf{e}_{qsq} = \mathbf{e}_q + \alpha\mathbf{S}_q\mathbf{e}_{sq} = \boldsymbol{\Omega}_{qsq}\mathbf{e}_q \\ \ddot{\mathbf{e}}_{qsq} = \mathbf{f}_{qsq} - \mathbf{f}_{qsq}^{dis} \end{cases}$$
$$\begin{cases} \mathbf{f}_{qsq} = \boldsymbol{\Omega}_{qsq}\mathbf{A}_n^{-1}\boldsymbol{\tau} \\ \mathbf{f}_{qsq}^{dis} = \boldsymbol{\Omega}_{qsq}\left(\mathbf{A}_n^{-1}\boldsymbol{\tau}^{dis} + \ddot{\mathbf{q}}^{ref}\right) \end{cases} \tag{13}$$

where $\mathbf{f}_{qsq}$ and $\mathbf{f}_{qsq}^{dis}$ stand for the control and disturbance inputs, respectively.

The dynamics of the coupled error in operation space $\mathbf{e}_{hsh}(\mathbf{e}_h, \mathbf{e}_{sh})$ could be obtained as

$$\begin{cases} \mathbf{e}_{hsh} = \mathbf{e}_h + \beta\mathbf{S}_h\mathbf{e}_{sh} = \boldsymbol{\Omega}_{hsh}\mathbf{e}_h \\ \ddot{\mathbf{e}}_{hsh} = \mathbf{f}_{hsh} - \mathbf{f}_{hsh}^{dis} \end{cases}$$
$$\begin{cases} \mathbf{f}_{hsh} = \boldsymbol{\Omega}_{hsh}\mathbf{A}_n^{-1}\boldsymbol{\tau} \\ \mathbf{f}_{hsh}^{dis} = \boldsymbol{\Omega}_{hsh}\left(\mathbf{J}\mathbf{A}_n^{-1}\boldsymbol{\tau}^{dis} - \dot{\mathbf{J}}\dot{\mathbf{q}} + \ddot{\mathbf{h}}^{ref}\right) \end{cases} \tag{14}$$

where $\mathbf{f}_{hsh}$ and $\mathbf{f}_{hsh}^{dis}$ stand for the control and disturbance inputs, respectively.

The dynamics (13) and (14) have the same form as error dynamics (7) - (10), thus the control for all these cases could be designed in the same way.

## III. CONTROL INPUT DESIGN

The dynamics of the motion tracking errors (7), the task tracking error (8), the cross-coupling synchronization errors in configuration (9) and operation (10) space, and the coupled errors (13) and (14) could all be written in the following form

$$\ddot{\mathbf{e}}_z = \mathbf{f}_z - \mathbf{f}_z^{dis} \tag{15}$$

Here the control error $\mathbf{e}_z$ takes values from the set $S_z = \left\{\mathbf{e}_q, \mathbf{e}_h, \mathbf{e}_{sq}, \mathbf{e}_{sh}, \mathbf{e}_{qsq}, \mathbf{e}_{hsh}\right\}$; the control input takes values from the set $F_z = \left\{\boldsymbol{\tau}_q, \mathbf{f}_h, \mathbf{f}_{sq}, \mathbf{f}_{sh}, \mathbf{f}_{qsq}, \mathbf{f}_{hsh}\right\}$ and the disturbance takes values from the set $F_z^{dis} = \left\{\boldsymbol{\tau}_q^{dis}, \mathbf{f}_h^{dis}, \mathbf{f}_{sq}^{dis}, \mathbf{f}_{sh}^{dis}, \mathbf{f}_{qsq}^{dis}, \mathbf{f}_{hsh}^{dis}\right\}$. The elements of the sets $S_z$, $F_z$, $F_z^{dis}$ are defined in corresponding equations (7) - (10), (13) and (14). The dynamics (15) describe the decoupled $n-$ double integrators with two inputs: the control $\mathbf{f}_z$ and the disturbance $\mathbf{f}_z^{dis}$.

The main goal of the design is to select a control input $\mathbf{f}_z$ that enforces the attractiveness and stability of the zero solution of the generalized error $\boldsymbol{\sigma}_z(\mathbf{e}_z, \dot{\mathbf{e}}_z)$. In equilibrium, $\boldsymbol{\sigma}_z(\mathbf{e}_z, \dot{\mathbf{e}}_z) = 0$ the relationship between $\mathbf{e}_z$ and $\dot{\mathbf{e}}_z$ is determined by the solution of the differential equation $\boldsymbol{\sigma}_z(\mathbf{e}_z, \dot{\mathbf{e}}_z) = 0$. This opens a range of possibilities in selecting $\boldsymbol{\sigma}_z(\mathbf{e}_z, \dot{\mathbf{e}}_z)$ such that specific requirements are met. Here generalized error $\boldsymbol{\sigma}_z(\mathbf{e}_z, \dot{\mathbf{e}}_z)$ is selected as a linear function:

$$\boldsymbol{\sigma}_z(\mathbf{e}_z, \dot{\mathbf{e}}_z) = \mathbf{C}_z\mathbf{e}_z + \dot{\mathbf{e}}_z;\ \boldsymbol{\sigma}_z \in \Re^{n\times 1}\mathbf{C}_z > 0 \tag{16}$$

For $\boldsymbol{\sigma}_z(\mathbf{e}_z, \dot{\mathbf{e}}_z) = 0$ the convergence rate of error $\mathbf{e}_z$ is defined by the design parameter $\mathbf{C}_z$ usually selected as a constant diagonal matrix.

From (15) and (16) the dynamics of the generalized error could be expressed as

$$\begin{aligned} \dot{\boldsymbol{\sigma}}_z &= \mathbf{f}_z - \mathbf{f}_z^{eq} \\ \mathbf{f}_z^{eq} &= \mathbf{f}_z^{dis} - \mathbf{C}_z\dot{\mathbf{e}}_z \end{aligned} \tag{17}$$

Here $\mathbf{f}_z^{eq}$ stands for the so-called equivalent control. For $\mathbf{f}_z = \mathbf{f}_z^{eq}$ the $\dot{\sigma}_z(\mathbf{e}_z, \dot{\mathbf{e}}_z) = 0$. To enforce the convergence to equilibrium the control input should have two terms. One to compensate for $\mathbf{f}_z^{eq}$ and another to enforce attractiveness and stability of $\boldsymbol{\sigma}_z(\mathbf{e}_z, \dot{\mathbf{e}}_z) = 0$. The attractiveness and stability

of the equilibrium $\boldsymbol{\sigma}_z(\mathbf{e}_z, \dot{\mathbf{e}}_z) = 0$ could be guaranteed if the Lyapunov function candidate and its derivative are selected as

$$\begin{cases} v_{lyz} = \dfrac{\boldsymbol{\sigma}_z^T \boldsymbol{\sigma}_z}{2} \\ \dot{v}_{lyz} = \boldsymbol{\sigma}_z^T \dot{\sigma}_z = -\boldsymbol{\sigma}_z^T \boldsymbol{\Psi}_z(\boldsymbol{\sigma}_z) < 0 \end{cases} \tag{18}$$

To satisfy (18) the components of the vector function $\boldsymbol{\Psi}_z(\boldsymbol{\sigma}_z)$ should have the same sign as the corresponding components of the generalized error, thus could be expressed as $\Psi_{zk}(\boldsymbol{\sigma}_z) = |\Psi_{zk}(\boldsymbol{\sigma}_z)| \operatorname{sgn}(\sigma_{zk}) k = 1, \ldots, n$. Such a selection of the components $\Psi_{zk}(\boldsymbol{\sigma}_z)$ yields the Lyapunov function derivative as in (19), thus the stability conditions are satisfied.

$$\begin{cases} \Psi_{zk}(\boldsymbol{\sigma}_z) = |\Psi_{zk}(\boldsymbol{\sigma}_z)| \operatorname{sgn}(\sigma_{zk}) \\ \dot{v}_{lyz} = -\boldsymbol{\sigma}_z^T \boldsymbol{\Psi}_z(\boldsymbol{\sigma}_z) \\ \dot{v}_{lyz} = -\sum_{k=1}^{k=n} |\Psi_{zk}(\boldsymbol{\sigma}_z)| |\sigma_{zk}| < 0 \end{cases} \tag{19}$$

The control input for dynamics (17) that enforce stability conditions (18) and (19) can be derived as

$$\mathbf{f}_z = \mathbf{f}_z^{eq} - \boldsymbol{\Psi}_z(\boldsymbol{\sigma}_z) \tag{20}$$

Plugging (20) into (17) yields the generalized error dynamics to

$$\dot{\sigma}_z + \boldsymbol{\Psi}_z(\boldsymbol{\sigma}_z) = 0 \tag{21}$$

The convergence is determined by the selection of the vector function $\boldsymbol{\Psi}_z(\boldsymbol{\sigma}_z)$. To demonstrate the variety of solutions in the selection of $\boldsymbol{\Psi}_z(\boldsymbol{\sigma}_z)$ below some of the possibilities are listed:

- $\boldsymbol{\Psi}_z(\boldsymbol{\sigma}_z) = \mathbf{K}_z \boldsymbol{\sigma}_z$, $\mathbf{K}_z > 0$ a positive definite diagonal matrix, yields asymptotic convergence to $\boldsymbol{\sigma}_z = 0$. The dynamics (21) becomes $\dot{\sigma}_z + \mathbf{K}_z \boldsymbol{\sigma}_z = 0$. By proper selection of design parameters $(\mathbf{C}_z, \mathbf{K}_z) > 0$ the asymptotic convergence to $\mathbf{e}_z = 0$ is guaranteed;
- $\boldsymbol{\Psi}_z(\boldsymbol{\sigma}_z) = Usgn(\boldsymbol{\sigma}_z), U > 0$ yields dynamics (21) as $\dot{\sigma}_z = -Usgn(\boldsymbol{\sigma}_z)$ and sliding mode motion is enforced [19], [22]. The control input is discontinuous, and chattering may occur in the system. After reaching the equilibrium $\boldsymbol{\sigma}_z = 0$ the convergence to $\mathbf{e}_z = 0$ is governed by $\mathbf{C}_z \mathbf{e}_z + \dot{\mathbf{e}}_z = 0$. The convergence rate and the stability of $\mathbf{e}_z = 0$ are guaranteed by the selection of the matrix $\mathbf{C}_z > 0$;
- finite-time convergence and sliding mode motion in the manifold $\boldsymbol{\sigma}_z = 0$ with continuous control could be realized by selecting $\boldsymbol{\Psi}_z(\boldsymbol{\sigma}_z) = \mathbf{K}_z \|\boldsymbol{\sigma}_z\|^{\rho} sign(\boldsymbol{\sigma}_z)$ with $0 < \rho < 1$ [22].

### A. APPLICATION OF THE EQUIVALENT CONTROL ESTIMATION

Implementation of control (20) requires information about $\mathbf{f}_z^{eq}$. For systems with uncertainties, the calculation $\mathbf{f}_z^{eq}$ is not practical. Instead, the estimation $\hat{\mathbf{f}}_z^{eq}$ could be used. The dynamics (17) has the same form as the plant dynamics (2) thus the design of the equivalent control observer could follow the same procedure as the design of the disturbance observer (3). Assuming the pair $(\boldsymbol{\sigma}_z, \mathbf{f}_z)$ is measured, the dynamics of the equivalent control is $\dot{f}_z^{eq} = 0$ and an auxiliary variable $\boldsymbol{\xi} = \mathbf{f}_z^{eq} + \mathbf{L}_z \boldsymbol{\sigma}_z$ of the equivalent control observer could be constructed as

$$\left.\begin{array}{c} \dot{\hat{\xi}} = -\mathbf{L}_z \hat{\xi} + \mathbf{L}_z (\mathbf{f}_z - \mathbf{L}_z \boldsymbol{\sigma}_z) \\ \hat{\mathbf{f}}_z^{eq} = \hat{\xi} - \mathbf{L}_z \boldsymbol{\sigma}_z \end{array}\right\} \dot{\hat{\mathbf{f}}}_z^{eq} + \mathbf{L}_z \hat{\mathbf{f}}_z^{eq} = \mathbf{L}_z \mathbf{f}_z^{eq} \tag{22}$$

Here $\mathbf{L}_z > 0$ is a diagonal positive definite matrix with elements $l_{zkk} > 0$. The observer (22) estimates the components of the equivalent control vector $\mathbf{f}_z^{eq}$. Using $\hat{\mathbf{f}}_z^{eq}$ instead of $\mathbf{f}_z^{eq}$ in control (20) yields the closed loop system dynamics to

$$\mathbf{f}_z = \hat{\mathbf{f}}_z^{eq} - \boldsymbol{\Psi}_z(\boldsymbol{\sigma}_z) \Rightarrow \begin{cases} \dot{\boldsymbol{\sigma}}_z + \boldsymbol{\Psi}_z(\boldsymbol{\sigma}_z) = \mathbf{p}_z\left(\hat{\mathbf{f}}_z^{eq}\right) \\ \dot{\hat{\mathbf{f}}}_z^{eq} + \mathbf{L}_z \hat{\mathbf{f}}_z^{eq} = \mathbf{L}_z \mathbf{f}_z^{eq} \\ \mathbf{p}_z\left(\hat{\mathbf{f}}_z^{eq}\right) = \hat{\mathbf{f}}_z^{eq} - \mathbf{f}_z^{eq} \end{cases} \tag{23}$$

Dynamics (23) describes an $2n-$ order system. If the separation of dynamics between observer and generalized error is realized then after reaching $p_z\left(\hat{\mathbf{f}}_z^{eq}\right) = 0$ the dynamics (23) becomes the same as the ideal one described in (21).

With $\Psi_{zk}(\boldsymbol{\sigma}_z) = |\Psi_{zk}(\boldsymbol{\sigma}_z)| sgn(\sigma_{zk})$ the control as in (23) yields the derivative of the Lyapunov function (18) as

$$\begin{cases} \mathbf{f}_z = \hat{\mathbf{f}}_z^{eq} - \boldsymbol{\Psi}_z(\boldsymbol{\sigma}_z) \\ \Psi_{zk}(\boldsymbol{\sigma}_z) = |\Psi_{zk}(\boldsymbol{\sigma}_z)| \operatorname{sgn}(\sigma_{zk}) \end{cases}$$
$$\dot{v}_{lyz} = \boldsymbol{\sigma}_z^T \dot{\sigma}_z = -\boldsymbol{\sigma}_z^T \left(\boldsymbol{\Psi}_z(\boldsymbol{\sigma}_z) - \mathbf{p}_z\left(\hat{\mathbf{f}}_z^{eq}\right)\right) \tag{24}$$

The derivative of the Lyapunov function could be expressed as

$$\dot{v}_{lyz} = -\sum_{k=1}^{k=n} \sigma_{zk} \left(\Psi_{zk}(\boldsymbol{\sigma}_z) - p_{zk}\left(\hat{\mathbf{f}}_z^{eq}\right)\right) \tag{25}$$

The separation of dynamics for the equivalent control estimation and the closed loop system the estimation error $p_z\left(\hat{\mathbf{f}}_z^{eq}\right) \to 0$ and all its components $p_{zk}\left(\hat{\mathbf{f}}_z^{eq}\right) \to 0, k = 1, \ldots, n$ faster than the components $\sigma_{zk}$. If $\boldsymbol{\Psi}_z(\boldsymbol{\sigma}_z)$ is selected such that $\operatorname{sgn}\left(\Psi_{zk}(\boldsymbol{\sigma}_z) - p_{zk}\left(\hat{\mathbf{f}}_z^{eq}\right)\right) = sgn\Psi_{zk}(\boldsymbol{\sigma}_z)$ then $\dot{v}_{lyz} < 0$ and the stability conditions are satisfied.

It is interesting to note that with a disturbance observer, (23) the control input $\mathbf{f}_z$ could be expressed as

$$\mathbf{f}_z = -\boldsymbol{\Psi}_z(\boldsymbol{\sigma}_z) - \mathbf{L}_z \int \left(\hat{\mathbf{f}}_z^{eq} - \mathbf{f}_z^{eq}\right) dt$$
$$\mathbf{f}_z = -\boldsymbol{\Psi}_z(\boldsymbol{\sigma}_z) - \mathbf{L}_z \int \left(\dot{\sigma}_z + \boldsymbol{\Psi}_z(\boldsymbol{\sigma}_z)\right) dt \tag{26}$$

The control $\mathbf{f}_z = \hat{\mathbf{f}}_z^{eq} - \boldsymbol{\Psi}_z(\boldsymbol{\sigma}_z)$ realizes an integral action in the closed loop system, by enforcing the $\hat{\mathbf{f}}_z^{eq} = \mathbf{f}_z^{eq}$ or $\dot{\sigma}_z = -\boldsymbol{\Psi}_z(\sigma_z)$.

The procedure shown in this section could be directly applied to control problems described in Section II with the appropriate selection of the error $\mathbf{e}_z$. This possibility to have structurally the same control error dynamics is a basis for the justification of the ways the design of the control may be applied to satisfy the cross-coupling requirements.

**TABLE 1. The design procedure and parameters.**

| | Design step & Equations | | Design Equation | Design parameter |
|---|---|---|---|---|
| 1 | System | (2) | $\mathbf{A}_n\ddot{\mathbf{q}} = \boldsymbol{\tau} - \boldsymbol{\tau}^{dis}$ | $\mathbf{A}_n$ |
| 2 | Observer design | (3) | $DOB: \{\boldsymbol{\tau}_q, \boldsymbol{\omega}, \mathbf{L}_q\} \rightarrow \hat{\boldsymbol{\tau}}_q^{dis}$ | $\mathbf{L}_q$ |
| 3 | Transformation | (9) | $\mathbf{e}_{sq} = \mathbf{T}_{sq}\mathbf{e}_q$ , $\mathbf{e}_{sh} = \mathbf{T}_{sh}\mathbf{e}_h$ | $\mathbf{T}_{sq}$ or $\mathbf{T}_{sh}$ |
| 4 | Error dynamics | (15) | $\ddot{\mathbf{e}}_z = \mathbf{f}_z - \mathbf{f}_z^{dis}$ | - |
| 5 | Generalized error | (16) | $\boldsymbol{\sigma}_z = \mathbf{C}_z\mathbf{e}_z + \dot{\mathbf{e}}_z$ | $\mathbf{C}_z$ |
| 6 | Convergence | (21) | $\dot{\boldsymbol{\sigma}}_z = -\boldsymbol{\Psi}_z(\boldsymbol{\sigma}_z)$ | $\boldsymbol{\Psi}_z(\boldsymbol{\sigma}_z)$ |
| 7 | Observer design | (22) | $DOB: \{\mathbf{f}_z, \boldsymbol{\sigma}_z, \mathbf{L}_z\} \rightarrow \hat{\mathbf{f}}_z^{eq}$ | $\mathbf{L}_z$ |
| 8 | Control input | (23) | $\mathbf{f}_z = \hat{\mathbf{f}}_z^{eq} - \boldsymbol{\Psi}_z(\boldsymbol{\sigma}_z)$ | - |

The key steps with equations used in the design procedure and the design parameters are summarized in Table 1.

The design procedure shows the key design parameters: the nominal inertia matrix $\mathbf{A}_n$, observer gain matrices $\mathbf{L}_q$, $\mathbf{L}_z$ and the generalized error gain $\mathbf{C}_z$ The observer gains are selected high with limitations related to the measurement noise. The matrix $\mathbf{C}_z$ depends on the desired bandwidth of the closed loop and the available control resources. Transformation matrices $\mathbf{T}_{sq}$ and $\mathbf{T}_{sh}$ must be regular.

The selection of the convergence term $\boldsymbol{\Psi}_z(\boldsymbol{\sigma}_z)$ determines the convergence of the generalized error. In most applications simple proportional term $\mathbf{K}_z\boldsymbol{\sigma}_z\mathbf{K}_z > 0$ is satisfactory. Selection of the discontinuous or fractional order $\boldsymbol{\Psi}_z(\boldsymbol{\sigma}_z) = \mathbf{K}_z \|\boldsymbol{\sigma}_z\|^{\rho} sign(\boldsymbol{\sigma}_z)$ term leads to motion in sliding mode and could be designed with predefined finite-time convergence.

### B. AN EXAMPLE OF 2 DOF SYSTEM

In [19] a design of the synchronization for 2-dof motion systems in operation space is realized using the Hadamard $\mathbf{H}_2$ projection matrix.

Here a 2-dof system (27) will be used as an example to demonstrate step-by-step application of the design procedure discussed in Section III. The nominal inertia matrix $\mathbf{A}_n$ is assumed diagonal, $a_{nkk} > 0, k = 1, 2$

$$\begin{cases} \mathbf{A}_n\ddot{\mathbf{q}} = \boldsymbol{\tau} - \boldsymbol{\tau}^{dis} \\ \boldsymbol{\tau}^{dis} = \mathbf{b}(\mathbf{q}, \dot{\mathbf{q}}) + \mathbf{g}(\mathbf{q}) + \boldsymbol{\tau}_{ext} + \Delta\mathbf{A}\ddot{\mathbf{q}} \\ \mathbf{q} = \begin{bmatrix} q_1 & q_2 \end{bmatrix}^T; \boldsymbol{\tau} = \begin{bmatrix} \tau_1 & \tau_2 \end{bmatrix}^T \end{cases} \tag{27}$$

If the disturbance $\boldsymbol{\tau}^{dis}$ is estimated then the control input $\boldsymbol{\tau} = \boldsymbol{\tau}^{con} + \hat{\tau}^{dis}$, with assumption that separation of dynamics is achieved, yields the compensated system dynamics as

$$\boldsymbol{\tau} = \boldsymbol{\tau}^{con} + \hat{\tau}^{dis} \Rightarrow \begin{cases} \mathbf{A}_n\ddot{\mathbf{q}} = \boldsymbol{\tau}^{con} - \mathbf{p}\left(\hat{\tau}^{dis}\right) \\ \mathbf{p}\left(\hat{\tau}^{dis}\right) = \left(\boldsymbol{\tau}^{dis} - \hat{\tau}^{dis}\right) \underset{t\rightarrow\infty}{\rightarrow} 0 \end{cases}$$

$$\mathbf{A}_n = \begin{bmatrix} a_{n11} & 0 \\ 0 & a_{n22} \end{bmatrix}; \begin{cases} \boldsymbol{\tau}_q^{con} = \begin{bmatrix} \tau_1^{con} & \tau_2^{con} \end{bmatrix}^T \\ \boldsymbol{\tau}^{dis} = \begin{bmatrix} \tau_1^{dis} & \tau_2^{dis} \end{bmatrix}^T \end{cases} \tag{28}$$

The reference motion $\mathbf{q}^{ref} = \begin{bmatrix} q_1^{ref} & q_2^{ref} \end{bmatrix}^T$ is assumed known. The motion tracking error $\mathbf{e}_q$, the cross-coupling synchronization error $\mathbf{e}_{sq}$, and the coupled error $\mathbf{e}_{qsq}$ are given as in (29) where $H_2$ is the Hadamard matrix.

$$\begin{aligned} \mathbf{e}_q &= \mathbf{q} - \mathbf{q}^{ref} \\ \mathbf{e}_{sq} &= \mathbf{H}_2\mathbf{e}_q = \mathbf{H}_2\mathbf{q} - \mathbf{H}_2\mathbf{q}^{ref} \\ \mathbf{e}_{qsq} &= \Omega_{qsq}\mathbf{e}_q;\ \Omega_{qsq} = \mathbf{I} + \alpha\mathbf{S}_q\mathbf{H}_2,\ \alpha > 0 \\ \mathbf{H}_2 &= \begin{bmatrix} 1 & 1 \\ 1 & -1 \end{bmatrix};\ \mathbf{S}_q = \begin{bmatrix} 1 & 0 \\ 0 & -1 \end{bmatrix}; \\ \boldsymbol{\Omega}_{qsq} &= \begin{bmatrix} 1+\alpha_1 & \alpha_1 \\ -\alpha_2 & 1+\alpha_2 \end{bmatrix} \end{aligned} \tag{29}$$

The dynamics of the errors (29) can be expressed as

$$\begin{cases} \mathbf{e}_q = \mathbf{q} - \mathbf{q}^{ref} \\ \mathbf{e}_{sq} = \mathbf{H}_2\mathbf{e}_q \\ \mathbf{e}_{qsq} = \boldsymbol{\Omega}_{qsq}\mathbf{e}_q \end{cases} \Rightarrow \begin{cases} \ddot{\mathbf{e}}_q = \boldsymbol{\tau}_q - \boldsymbol{\tau}_q^{dis} \\ \ddot{\mathbf{e}}_{sq} = \mathbf{f}_{sq} - \mathbf{f}_{sq}^{dis} \\ \ddot{\mathbf{e}}_{qsq} = \mathbf{f}_{qsq} - \mathbf{f}_{qsq}^{dis} \end{cases} \tag{30}$$

Here the control inputs $\boldsymbol{\tau}_q, \mathbf{f}_{sq}\mathbf{f}_{qsq}$ and disturbances $\boldsymbol{\tau}_q^{dis}$, $\mathbf{f}_{sq}^{dis}$ and $\mathbf{f}_{qsq}^{dis}$ are given as

$$\begin{cases} \tau_q = \begin{cases} \mathbf{A}_n^{-1}\boldsymbol{\tau} & \text{for dynamics (27)} \\ \mathbf{A}_n^{-1}\boldsymbol{\tau}^{con} & \text{for dynamics (28)} \end{cases} \\ \boldsymbol{\tau}_q^{dis} = \begin{cases} \mathbf{A}_n^{-1}\boldsymbol{\tau}^{dis} + \ddot{\mathbf{q}}^{ref} & \text{for dynamics (27)} \\ \mathbf{A}_n^{-1}\mathbf{p}\left(\hat{\tau}^{dis}\right) + \ddot{\mathbf{q}}^{ref} & \text{for dynamics (28)} \end{cases} \end{cases}$$

$$\begin{cases} \mathbf{f}_{sq} = \mathbf{H}_2\boldsymbol{\tau}_q \\ \mathbf{f}_{sq}^{dis} = \mathbf{H}_2\boldsymbol{\tau}_q^{dis} \end{cases} \quad \begin{cases} \mathbf{f}_{qsq} = \boldsymbol{\Omega}_{qsq}\boldsymbol{\tau}_q \\ \mathbf{f}_{qsq}^{dis} = \boldsymbol{\Omega}_{qsq}\boldsymbol{\tau}_q^{dis} \end{cases} \tag{31}$$

The corresponding generalized error $\boldsymbol{\sigma}_q, \boldsymbol{\sigma}_{sq}, \boldsymbol{\sigma}_{qsq}$ and their derivatives could be written as

$$\begin{cases} \boldsymbol{\sigma}_q = \dot{\mathbf{e}}_q + \mathbf{C}_q\mathbf{e}_q;\ \mathbf{C}_q > 0 \\ \boldsymbol{\sigma}_h = \dot{\mathbf{e}}_h + \mathbf{C}_h\mathbf{e}_h;\ \mathbf{C}_h > 0 \\ \boldsymbol{\sigma}_{qsq} = \dot{\mathbf{e}}_{qsq} + \mathbf{C}_{qsq}\mathbf{e}_{qsq};\ \mathbf{C}_{qsq} > 0 \end{cases} \quad \begin{cases} \dot{\sigma}_q = \boldsymbol{\tau}_q - \boldsymbol{\tau}_q^{eq} \\ \dot{\sigma}_{sq} = \mathbf{f}_{sq} - \mathbf{f}_{sq}^{eq} \\ \dot{\sigma}_{qsq} = \mathbf{f}_{qsq} - \mathbf{f}_{qsq}^{eq} \end{cases} \tag{32}$$

Here the equivalent control input is defined as

$$\begin{aligned} \boldsymbol{\tau}_q^{eq} &= \begin{cases} \mathbf{A}_n^{-1}\boldsymbol{\tau}^{dis} + \ddot{\mathbf{q}}^{ref} & \text{for dynamics (27)} \\ \mathbf{A}_n^{-1}\mathbf{p}\left(\hat{\tau}^{dis}\right) + \ddot{\mathbf{q}}^{ref} - \mathbf{A}_n^{-1}\mathbf{C}_q\dot{\mathbf{e}}_q & \text{for dynamics (28)} \end{cases} \\ \mathbf{f}_{sq}^{eq} &= \mathbf{H}_2\boldsymbol{\tau}_q^{eq} \\ \mathbf{f}_{qsq}^{eq} &= \boldsymbol{\Omega}_{qsq}\boldsymbol{\tau}_q^{eq} \end{aligned} \tag{33}$$

The equivalent control $\boldsymbol{\tau}_q^{eq}$, $\mathbf{f}_{sq}^{eq}$ and $\mathbf{f}_{qsq}^{eq}$ could be estimated by the observer (22) with an appropriate change of coordinates. Application of control as in (23) yields the closed-loop motion as

$$\begin{aligned} \boldsymbol{\tau}_q &= \hat{\boldsymbol{\tau}}_q^{eq} - \mathbf{K}_q\boldsymbol{\sigma}_q \Rightarrow \dot{\sigma}_q + \mathbf{K}_q\boldsymbol{\sigma}_q = \hat{\boldsymbol{\tau}}_q^{eq} - \boldsymbol{\tau}_q^{eq} \\ \mathbf{f}_{sq} &= \hat{\mathbf{f}}_{sq}^{eq} - \mathbf{K}_{sq}\boldsymbol{\sigma}_{sq} \Rightarrow \dot{\sigma}_{sq} + \mathbf{K}_{sq}\boldsymbol{\sigma}_{sq} = \hat{\mathbf{f}}_{sq}^{eq} - \mathbf{f}_{sq}^{eq} \\ \mathbf{f}_{qsq} &= \hat{\mathbf{f}}_{qsq}^{eq} - \mathbf{K}_{qsq}\boldsymbol{\sigma}_{qsq} \Rightarrow \dot{\sigma}_{qsq} + \mathbf{K}_{qsq}\boldsymbol{\sigma}_{qsq} = \hat{\mathbf{f}}_{qsq}^{eq} - \mathbf{f}_{qsq}^{eq} \end{aligned} \tag{34}$$

Another possibility is to combine the control inputs $\boldsymbol{\tau}_q$ and $\mathbf{f}_{sq}$ instead of the control errors $\mathbf{e}_q$ and $\mathbf{e}_{sq}$. In this case the coupled control input is expressed as

$$\boldsymbol{\tau} = \boldsymbol{\tau}_q + \lambda \mathbf{A}_n \mathbf{H}_4^{-1} \mathbf{f}_{sq} \tag{35}$$

The parameter $\lambda$ defines the relative weight of the synchronization control input $\mathbf{f}_{sq}$. Control (35) introduces redundancy into the overall structure and, as will be shown in simulation and experiments, a system with such control could tolerate a loss of some controller-generating components of the vector $\boldsymbol{\tau}_q$.

The design parameters for the 2-dof system design are:

(i) the gains in the disturbance $l_{1\tau}$, $l_{2\tau}$ and equivalent control observers $l_{1e}$, $l_{2e}$. These parameters depend on the measurement noise and the desired bandwidth of the closed-loop system;

(ii) the components of the generalized error gain matrix $\mathbf{C}_q, \mathbf{C}_{sq}, \mathbf{C}_{qsq}$ define the convergence rate of the control error to the equilibrium $\mathbf{e}_q = 0, \mathbf{e}_{sq} = 0$, and $\mathbf{e}_{qsq} = 0$. Their selection depends on the desired closed-loop bandwidth;

(iii) the feedback gains $\mathbf{K}_q, \mathbf{K}_{sq}, \mathbf{K}_{qsq}$ define the convergence to the equilibrium $\boldsymbol{\sigma}_q = 0, \boldsymbol{\sigma}_{sq} = 0$, and $\boldsymbol{\sigma}_{qsq} = 0$. Together with generalized error gains the choice of $\mathbf{K}_q, \mathbf{K}_{sq}, \mathbf{K}_{qsq}$ defining the ''stiffness'' of the closed-loop control.

(iv) the gains $\alpha$, $\beta$ and $\lambda$ define the weight of the synchronization error and control. In our experiments $\alpha$, $\beta$, $\lambda < 1$ are used.

(v) The choice of the cross-coupling matrix $\mathbf{H}$ is restricted to the full-rank matrices. One way of derivation of the transformation matrix $\mathbf{H}$ if direct construction of Hadamard matrix is not feasible is shown in [23]. In general, any regular matrix could be used.

The structure of the system is shown in Figure 1. (a)-(c). The operation space control with synchronization error $\mathbf{e}_{sq} = H_2\mathbf{e}_q$ and the synchronization controller with structure with $\mathbf{f}_{sq}$ is depicted in Fig. 1. (a). The system with coupled error $\mathbf{e}_{qsq} = \boldsymbol{\Omega}_{qsq}\mathbf{e}_q$ and control $\mathbf{f}_{sq}$ is depicted in Fig. 1. (b). In Fig. 1. (c) the combination of the motion tracking and the synchronization at the control input level is shown.

## IV. SIMULATION AND EXPERIMENTAL VERIFICATION

In simulation and experimental verification of the proposed algorithms, a four-axis system is used with DC motors as actuators. The parameters of actuators are shown in Table 2. The interaction with the environment (represented by external force in the mathematical model) is treated as a disturbance. In both simulation and experiments, the motor torque is treated as the control input. The estimation of the disturbance is realized for each axis separately. The nominal motor parameters are used in the control design.

The task is defined as the synchronization of the trajectory tracking. The motion tracking errors $e_{qk} = q_k - q_k^{ref}$ $k = 1, \ldots, 4$ and motion references $q_k^{ref}(t)$ are, in simulation and experiments, selected as constants or sinusoidal defined as $e_{q1}$

$$\underbrace{\begin{bmatrix} e_{q1} \\ e_{q2} \\ e_{q3} \\ e_{q4} \end{bmatrix}}_{\mathbf{e}_q} = \underbrace{\begin{bmatrix} q_1 \\ q_2 \\ q_3 \\ q_4 \end{bmatrix}}_{\mathbf{q}} - \underbrace{\begin{bmatrix} q_1^{ref} \\ q_2^{ref} \\ q_3^{ref} \\ q_4^{ref} \end{bmatrix}}_{\mathbf{q}^{ref}};$$

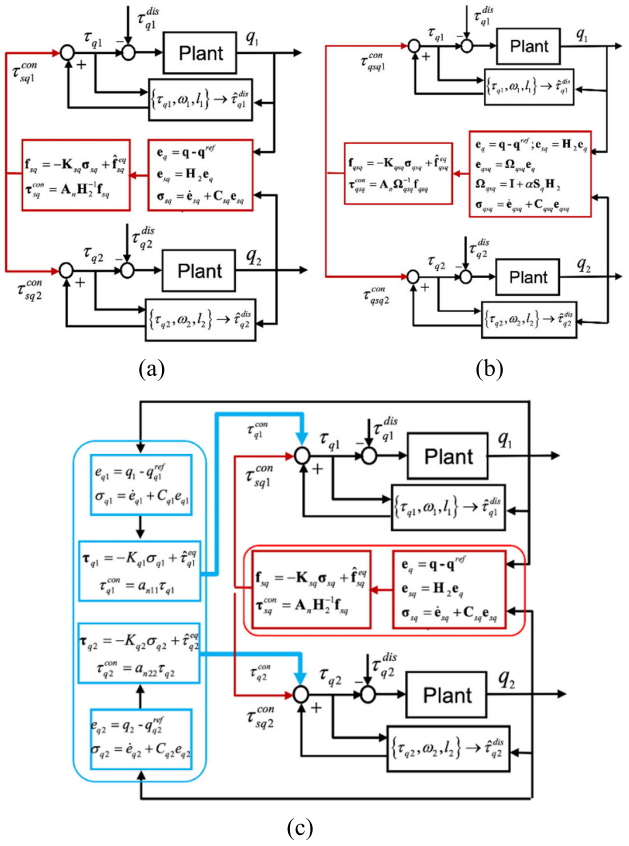


**FIGURE 1.** The structure of the 2-dof synchronization system: (a) synchronization task control; (b) cross-coupling coupled-error synchronization (c) the coupled control input synchronization control.

**TABLE 2.** The data on DC motors.

| Parameter | Symbol | Value |
|---|---|---|
| Motor Type | 2642W012CR | |
| Supply voltage | $V_a$ | 12 V |
| Max. Supply current | $I_a$ | 2 A |
| Moment of inertia | $J$ | $10^{-3}$ kgm$^2$ |
| Inductance | $L_a$ | 130 μH |
| Resistance | $R_a$ | 1.420 Ω |
| Motor nominal speed | $\omega_n$ | 12.65 rad/s |
| Gear ratio | G | 43 |
| Encoder | IE2-512 | 512 Lines/rev |
| Motor driver | MCDC3006S | |
| Sampling frequency | 35 kHz | |

$$\underbrace{\begin{bmatrix} q_1^{ref} \\ q_2^{ref} \\ q_3^{ref} \\ q_4^{ref} \end{bmatrix}}_{\mathbf{q}^{ref}} = \begin{bmatrix} 1 \\ 2 \\ 3 \\ 4 \end{bmatrix} \; or \; \begin{bmatrix} 1 \\ 2 \\ 3 \\ 4 \end{bmatrix} \sin(0.2\pi t) \tag{36}$$

The cross-coupling synchronization error is defined as in (37) with $\mathbf{e}_{sq} = \mathbf{H}_4 \mathbf{e}_q$ where $\mathbf{H}_4$ is given as

$$\underbrace{\begin{bmatrix} e_{sq1} \\ e_{sq2} \\ e_{sq3} \\ e_{sq4} \end{bmatrix}}_{\mathbf{e}_{sq}} = \underbrace{\begin{bmatrix} 1 & 1 & 1 & 1 \\ 1 & -1 & 1 & -1 \\ 1 & 1 & -1 & -1 \\ 1 & -1 & -1 & 1 \end{bmatrix}}_{\mathbf{H}_4} \underbrace{\begin{bmatrix} e_{q1} \\ e_{q2} \\ e_{q3} \\ e_{q4} \end{bmatrix}}_{\mathbf{e}_q} \tag{37}$$

The simulation and experiments are aimed to show the following control system features:

- the behavior of the system without and with cross-coupling synchronization control;
- the behavior of the system if the cross-coupling synchronization control is combined with motion tracking control by coupled error (11) (system structure as depicted in Fig 1. (b) for 2nd order system);
- the behavior of the system if the cross-coupling synchronization control is integrated with motion tracking control by coupled control (35) (system structure as depicted in Fig. 1 (c) for 2nd order system).

### A. SIMULATION OF A 4-DOF SYSTEM

Simulations are conducted in a Matlab/Simulink environment. The simulation experiments are implemented under the following conditions:

#### 1) EXPERIMENTS WITHOUT SYNCHRONIZATION

- the structure of the disturbance observer for each axis as shown in (3) $DOB : \{\tau_{qk}, \omega_k, L_{qk}\} \rightarrow \hat{\tau}_{qk}^{dis}$, $k = 1, \ldots, 4$;
- the motion tracking errors $e_{qk} = q_k - q_k^{ref}$, $k = 1, \ldots, 4$ are calculated as in (36). The generalized errors for each axis are calculated as in (32) with $\sigma_{qk} = \dot{e}_{qk} + C_{qk} e_{qk}$;
- the equivalent control is estimated for each axis using the observer as (22) $DOB : \{\tau_{qk}, \sigma_{qk}, L_{qzk}\} \rightarrow \hat{\tau}_{qk}^{eq}$ $k = 1, \ldots, 4$;
- the motion tracking control input is calculated for each axis as in (23), $\tau_{qk} = \hat{\tau}_{qk}^{eq} - K_{qk}\sigma_{qk}.; k = 1, \ldots, 4$.

#### 2) EXPERIMENTS WITH CROSS-COUPLING SYNCHRONIZATION

- the components of the synchronization error $\mathbf{e}_{sq} = H_4 \mathbf{e}_q$ are calculated using transformation (37). The generalized errors are calculated as in (32) with $\sigma_{sqk} = \dot{e}_{sqk} + C_{sqk} e_{sqk}$, $k = 1, \ldots, 4$.
- the equivalent control is estimated for each axis using observer as in (22) $DOB : \{f_{sqk}, \sigma_{sqk}, L_{sqzk}\} \rightarrow \hat{f}_{sqk}^{eq}$ with, $k = 1, \ldots, 4$.

#### 3) EXPERIMENTS WITH CROSS-COUPLING SYNCHRONIZATION ERROR

- the components of the coupled error $\mathbf{e}_{qsq} = \mathbf{\Omega}_{qsq} \mathbf{e}_q$ are determined using transformation $\mathbf{\Omega}_{qsq} = I + \alpha S_q H_4$, and $H_4$ as in (37), $S_q = diag\,(1, -1, -1, 1)$;
- the equivalent control is estimated for each axis using observer as in (22) $DOB : \{f_{qsqk}, \sigma_{qsqk}, L_{qsqk}\} \rightarrow \hat{f}_{qsqk}^{eq}$ with, $k = 1, \ldots, 4$.

#### 4) EXPERIMENTS WITH COUPLING SYNCHRONIZATION CONTROL

- the control $\boldsymbol{\tau}_q$ and synchronization control $\mathbf{f}_{sq}$ are calculated as shown in A: and B: above. The coupling of these two controls is realized by $\boldsymbol{\tau} = \boldsymbol{\tau}_q + \lambda \mathbf{A}_n \mathbf{H}_4^{-1} \mathbf{f}_{sq}$.

In all simulation experiments, the control input is not limited. This solution is adopted to show the ideal behavior and compare the transients with ones obtained in the experimental system in which the input is limited by the allowed current delivered from the driver.

**TABLE 3. The design parameters used in simulation and experiments.**

| | Design step & Equations | Parameter | Axis #1 | Axis #2 | Axis #3 | Axis #4 |
|---|---|---|---|---|---|---|
| 1 | System (2) | $\mathbf{A}_n$ | $10^{-3}$ kgm$^2$ | $10^{-3}$ kgm$^2$ | $10^{-3}$ kgm$^2$ | $10^{-3}$ kgm$^2$ |
| 2 | Observer (3) | $\mathbf{L}_q$ | 2500 | 2500 | 2500 | 2500 |
| 3 | Transform (9) | $\mathbf{H}_4$ | $\mathbf{H}_4$ | $\mathbf{H}_4$ | $\mathbf{H}_4$ | $\mathbf{H}_4$ |
| 4 | Error (16) in simulation | $\mathbf{C}_z$ | 250 | 100 | 250 | 330 |
| 5 | Conv. gain (21) in experiments | $\mathbf{K}_z$ | 6.5 | 6.5 | 6.5 | 6.5 |
| 6 | Observer (22) | $\mathbf{L}_z$ | 2500 | 2500 | 2500 | 2500 |
| 7 | Error (13) | $\alpha$ | 0.8 | 0.8 | 0.8 | 0.8 |
| 8 | Control | $\lambda$ | 0.8 | 0.8 | 0.8 | 0.8 |

The parameters used in the simulation and experiments are shown in Table 3. Note that elements of the matrix $\mathbf{C}_z$ are not kept equal. That is visible in the upper graph in Fig. 2 (motion without synchronization) by examining the settling time. Such parameters are selected to emphasize the influence of the convergence term in forcing equal settling time in all axes (lower diagram in Fig. 2.). Due to the limits on the control, this effect is less emphasized in experimental results depicted in Fig. 6. The settling time is given in Table 4.

In Fig. 2 motion errors for system transients for starting from zero initial condition to constant references defined in (36) are shown. The upper diagram is for systems without cross-coupling and the lower diagrams show transients with coupled error (13). The simultaneous convergence in the case of cross-coupling synchronization is clear.

The transients for synchronization control with coupled control input $\boldsymbol{\tau} = \boldsymbol{\tau}_q + \lambda \mathbf{A}_n \mathbf{H}_4^{-1} \mathbf{f}_{sq}$ are depicted in Fig. 3. The convergence from zero initial conditions to reference motion and the failure of motion tracking in the axis $q_1$ at $t = 2.51s$ are shown. The operation of the system and recovery of the

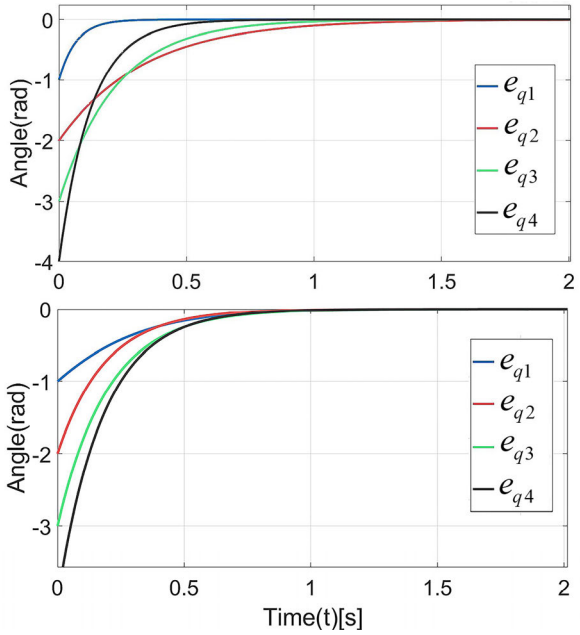


**FIGURE 2.** The motion tracking error without (upper diagram) and with cross-coupling synchronization (lower diagram).

**TABLE 4.** The settling time in simulation and experiments.

| Parameter | Unit | Axis | | | |
|---|---|---|---|---|---|
| | | #1 | #2 | #3 | #4 |
| **Transients without synchronization (simulation)** | | | | | |
| Settling time | $t_s$ [s] | 0.36 | 1.82 | 1.65 | 0.85 |
| **Transients without synchronization (experiments)** | | | | | |
| Settling time | $t_s$ [s] | 1.02 | 1.25 | 1.65 | 2.23 |
| **Transients with synchronization (simulation)** | | | | | |
| Settling time | $t_s$ [s] | 1.22 | 1.22 | 1.22 | 1.22 |
| **Transients with synchronization (experiments)** | | | | | |
| Settling time | $t_s$ [s] | 1.56 | 1.56 | 1.57 | 1.56 |

synchronization is clear, which confirms the redundancy in the selected control system structure.

The steady state errors in simulation and experiments are given in Table 5.

The transients from zero initial conditions and zero crossing for the system with sinusoidal references (36) are shown in Fig. 4.

Simulation results illustrate the functionality and salient features of the proposed design. They confirm the desired behavior with both coupled errors and coupled control cases. The loss of one of the controllers in the motion control loop and the re-establishment of the synchronization as shown in Fig. 2 confirms a redundancy property of the proposed design.

### B. EXPERIMENTAL RESULTS FOR 4 DOF SYSTEM

The experimental validation of the proposed design is conducted on a set-up consisting of four actuators as shown in Fig. 5. The control algorithms are implemented in the dSPACE environment with the DS1005 as a controller card, DS3001 encoder card, and DAC card DS2103. The sampling interval in all experiments is kept constant $T = 28.5\mu s$.

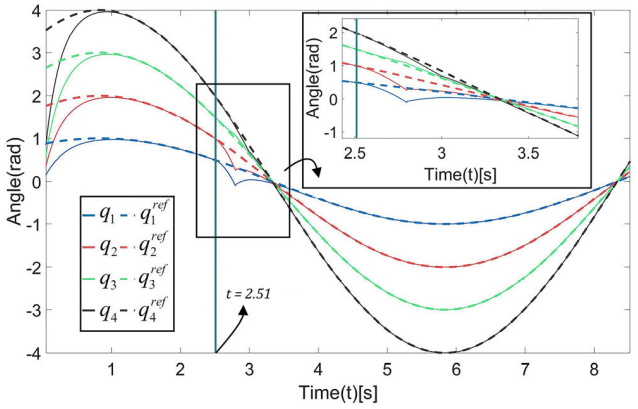


**FIGURE 3.** The motion tracking and simulated loss of the motion tracking controller for $q_1$ at $t = 2.51s$.

**TABLE 5.** The steady-state error in simulation and experiments.

| Parameter | Unit | Axis | | | |
|---|---|---|---|---|---|
| | | #1 | #2 | #3 | #4 |
| **Transients without synchronization (simulation)** | | | | | |
| Steady-state error | $e_{ss}$ [rad] | $6\cdot10^{-5}$ | $5.1\cdot10^{-5}$ | $4.5\cdot10^{-5}$ | $4\cdot10^{-5}$ |
| **Transients without synchronization (experiments)** | | | | | |
| Steady-state error | $e_{ss}$ [rad] | $4\cdot10^{-5}$ | $4.1\cdot10^{-5}$ | $3.5\cdot10^{-5}$ | $3.3\cdot10^{-5}$ |
| **Transients with synchronization (simulation)** | | | | | |
| Steady-state error | $e_{ss}$ [rad] | $5.1\cdot10^{-5}$ | $5\cdot10^{-5}$ | $4.1\cdot10^{-5}$ | $3\cdot10^{-5}$ |
| **Transients with synchronization (experiments)** | | | | | |
| Steady-state error | $e_{ss}$ [rad] | $3\cdot10^{-5}$ | $3.2\cdot10^{-5}$ | $2.5\cdot10^{-5}$ | $2.3\cdot10^{-5}$ |

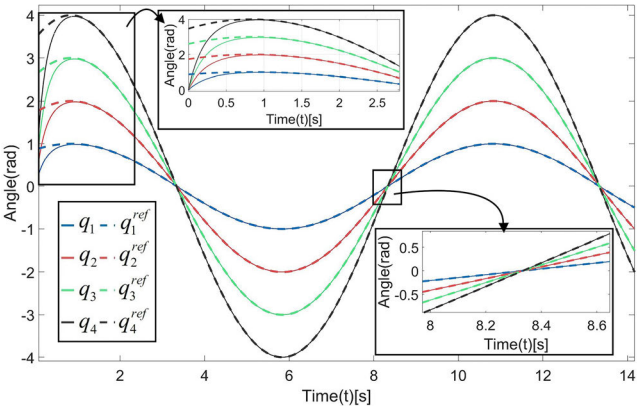


**FIGURE 4.** The synchronization of the motion with sinusoidal references of different amplitudes.

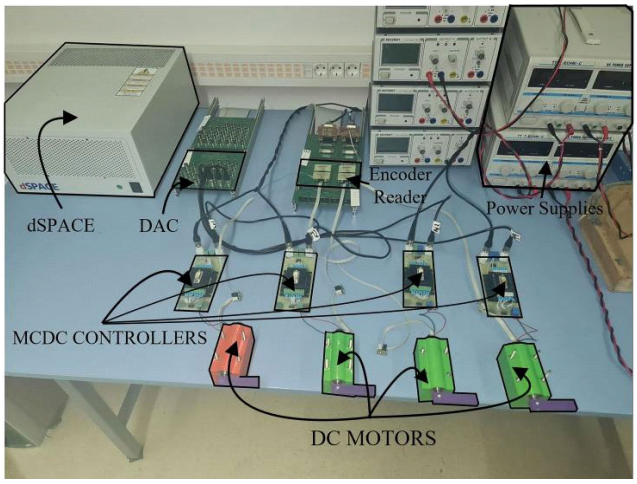


**FIGURE 5.** The setup used for the experimental verification of the proposed design.

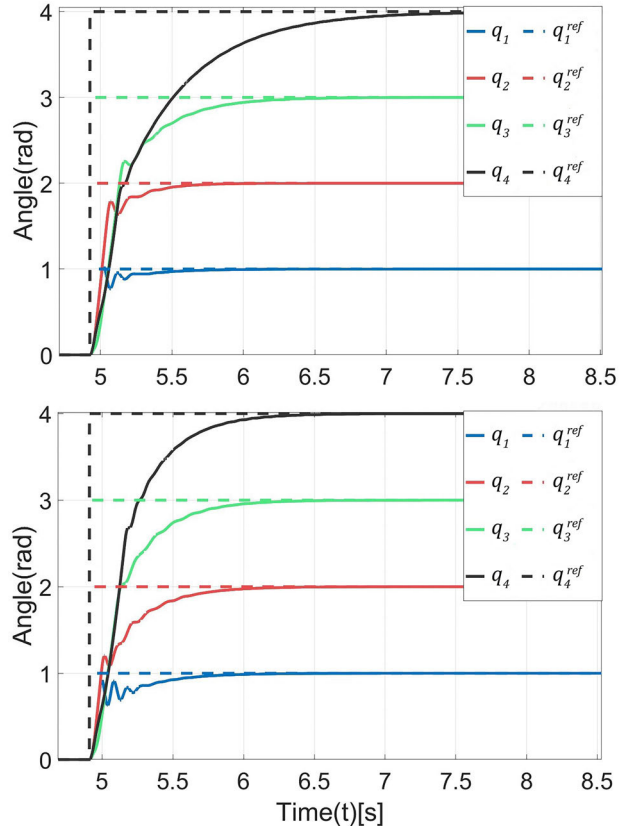


**FIGURE 6.** The motion tracking without (upper diagram) and with (lower diagram) cross-coupling synchronization for constant references.

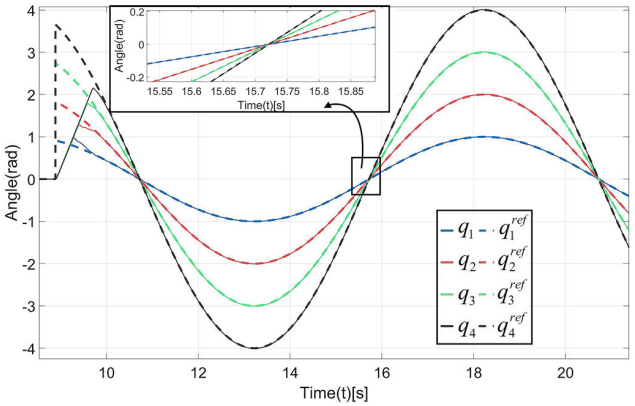


**FIGURE 7.** Cross-coupling synchronization control for sinusoidal references.

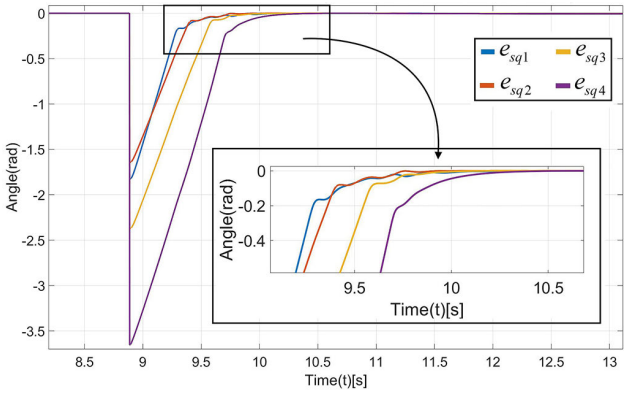


**FIGURE 8.** The synchronization error for the experiment shown in Fig. 7.

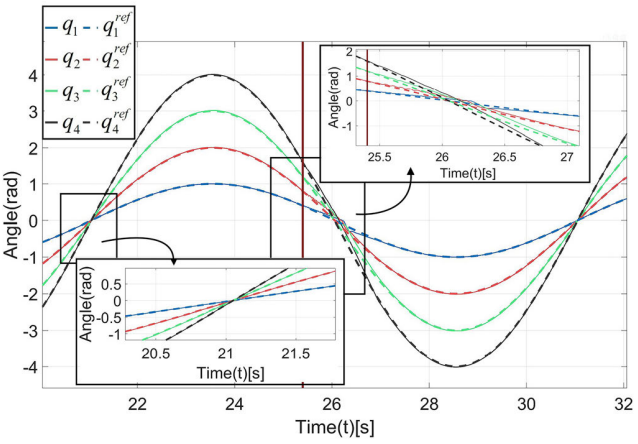


**FIGURE 9.** The trajectory evolution for sinusoidal references and the motion controller loss for the actuator $q_1$ at $t = 25.1s$.

The experiments are implemented for the same references and controller parameters as the corresponding simulation. The key difference between experimental and simulation is the limit of the control input applied in the experiments which has not been applied in simulation. That could be detected in the initial transients or transients with large errors that caused control saturation.

In Fig. 6 the transients from zero initial conditions to a constant reference with and without cross-coupling synchronization are shown (the synchronization control is realized with coupling error $\mathbf{e}_{qsq} = \mathbf{\Omega}_{qsq}\mathbf{e}_q$). Transients depicted in Fig. 6 illustrate the validity of the proposed algorithm and the consistency of the simulation and experimental results.

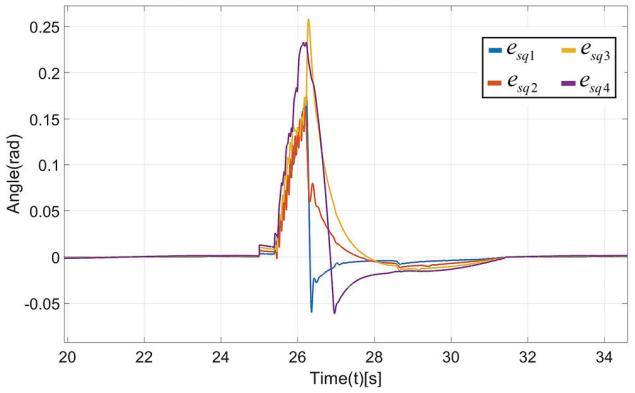


**FIGURE 10.** The changes of the synchronization error in the experiment shown in Fig. 9.

In Fig. 7 the cross-coupling synchronization with coupling control $\boldsymbol{\tau} = \boldsymbol{\tau}_q + \lambda A_n H_4^{-1} \mathbf{f}_{sq}$ is shown. The synchronous zero crossing for all axes is shown.

The augmented synchronization error for the reaching stage from zero initial conditions is shown in Fig. 8. The straight-line motion in all axes is due to saturation of the control torque and consequently saturation of the motor speed.

The zero crossing and the evolution of system behavior in the malfunction of one of the motion controllers are depicted in Fig. 9. This experiment is conducted under the same conditions (different time windows) as the one shown in Fig. 7. Here malfunction of the controller in the axis $q_1$ appears at $t = 25.1s$. In the zoomed part the effect on the zero crossing for all four actuators is shown. The changes in the synchronization error in the same experiment are depicted in Fig. 10.

The simulation and experimental results demonstrate the validity of the proposed algorithm and the effectiveness of its usage.

## V. CONCLUSION

In this paper, a framework for the design of the cross-coupled motion synchronization control for uncertain multi-axis systems is discussed in detail. The proposed design could be applied in different configurations: (i) as a motion (position or speed) or task tracking control design, (ii) as a cross-coupling synchronization controller in which the synchronization is enforced by setting a functional relationship between system states; (iii) a combination of the motion tracking and error based cross-coupling control. The proposed formulation allows controller design that will enforce the desired convergence of the generalized error while keeping the same structure of the controller. Specific application of the unknown input observer within the controller allows efficient application for uncertain systems. The simulation and experimental results verify the effectiveness of the proposed algorithm. Further research in this framework may include the selection of the structure of generalized error and the convergence term $\boldsymbol{\Psi}_z(\boldsymbol{\sigma}_z)$ to enforce predefine finite-time convergence of the control error, the implementation of different observers and adaptation for the changes in the nominal inertia matrix. Interesting work would be the extension to the compliant control systems.

## REFERENCES

[1] H. Dou, "Lyapunov approach for motion synchronization of a two-slider system," *Trans. Inst. Meas. Control*, vol. 41, no. 14, pp. 4063–4072, Oct. 2019.
[2] D. Sun, X. Shao, and G. Feng, "A model-free cross-coupled control for position synchronization of multi-axis motions: Theory and experiments," *IEEE Trans. Control Syst. Technol.*, vol. 15, no. 2, pp. 306–314, Mar. 2007.
[3] M. Wang, X. Ren, and Q. Chen, "Robust tracking and distributed synchronization control of a multi-motor servomechanism with H-infinity performance," *ISA Trans.*, vol. 72, pp. 147–160, Jan. 2018.
[4] Y.-T. Shih, C.-S. Chen, and A.-C. Lee, "A novel cross-coupling control design for bi-axis motion," *Int. J. Mach. Tools Manuf.*, vol. 42, no. 14, pp. 1539–1548, Nov. 2002.
[5] B. Sencer, T. Mori, and E. Shamoto, "Design and application of a sliding mode controller for accurate motion synchronization of dual servo systems," *Control Eng. Pract.*, vol. 21, no. 11, pp. 1519–1530, Nov. 2013.
[6] K. Dai, Z. Zhu, Y. Tang, G. Shen, X. Li, and Y. Sa, "Position synchronization tracking of multi-axis drive system using hierarchical sliding mode control," *J. Brazilian Soc. Mech. Sci. Eng.*, vol. 43, no. 4, pp. 1–16, Apr. 2021.
[7] M. H. Cheng, Y. J. Li, and E. G. Bakhoum, "Controller synthesis of tracking and synchronization for multiaxis motion system," *IEEE Trans. Control Syst. Technol.*, vol. 22, no. 1, pp. 378–386, Jan. 2014.
[8] Z. Liu, W. Lin, X. Yu, J. J. Rodríguez-Andina, and H. Gao, "Approximation-free robust synchronization control for dual-linear-motors-driven systems with uncertainties and disturbances," *IEEE Trans. Ind. Electron.*, vol. 69, no. 10, pp. 10500–10509, Oct. 2022.
[9] C.-S. Chen and L.-Y. Chen, "Robust cross-coupling synchronous control by shaping position commands in multiaxes system," *IEEE Trans. Ind. Electron.*, vol. 59, no. 12, pp. 4761–4773, Dec. 2012.
[10] Z. Liu, J. Chen, and K. Zhang, "New hydraulic synchronization system based on fuzzy PID control strategy," in *Advanced Materials Research*. Wollerau, Switzerland: Trans Tech Publications, Sep. 2013.
[11] C. Lin, W. Chu, and W. Gai, "Research on the synchronization motion control technology for multi-axis system," in *Proc. IEEE Inf. Technol., Netw., Electron. Autom. Control Conf.*, May 2016, pp. 672–679.
[12] S. Guo, Z. Ma, L. Li, Z. Liu, and P. Huang, "Predefined-time sensorless admittance tracking control for teleoperation systems with error constraint and personalized compliant performance," *IEEE Trans. Ind. Electron.*, early access, Jun. 26, 2023, doi: 10.1109/TIE.2023.3288169.
[13] Z. Ma, D. Shi, Z. Liu, J. Yu, and P. Huang, "A bilateral teleoperation system with learning-based cognitive guiding force," *IEEE Trans. Cogn. Develop. Syst.*, early access, Feb. 15, 2023, doi: 10.1109/TCDS.2023.3245216.
[14] Q. V. Doan, T. D. Le, and A. T. Vo, "Synchronization full-order terminal sliding mode control for an uncertain 3-DOF planar parallel robotic manipulator," *Appl. Sci.*, vol. 9, no. 9, p. 1756, Apr. 2019.
[15] G. Zhong, Z. Shao, H. Deng, and J. Ren, "Precise position synchronous control for multi-axis servo systems," *IEEE Trans. Ind. Electron.*, vol. 64, no. 5, pp. 3707–3717, May 2017.
[16] Y.-W. Wang, A. Liu, W.-A. Zhang, and M. Wu, "Synchronization tracking control of networked multi-axis motion systems: A cooperative distributed model predictive control approach," *Control Eng. Pract.*, vol. 126, Sep. 2022, Art. no. 105233.
[17] Z. Liu, W. Chen, K. Jin, and H. Li, "Task-space trajectory tracking control for coordinated manipulation using sampled coupling data," *IEEE Robot. Autom. Lett.*, vol. 6, no. 4, pp. 8434–8441, Oct. 2021.
[18] F. He and C. Wang, "Cross-coupling synchronous control of dual-motor networked motion control system," in *Proc. 36th Chin. Control Conf. (CCC)*, Jul. 2017, pp. 7628–7633.
[19] A. Šabanović and K. Ohnishi, *Motion Control Systems*. Hoboken, NJ, USA: Wiley, 2011.
[20] A. Shimada, *Disturbance Observer for Advanced Motion Control With MATLAB/Simulink* (IEEE Press Series on Control Systems Theory and Applications). Hoboken, NJ, USA: Wiley, 2023.

[21] X. Yang, W. Deng, and J. Yao, "Neural adaptive dynamic surface asymptotic tracking control of hydraulic manipulators with guaranteed transient performance," *IEEE Trans. Neural Netw. Learn. Syst.*, vol. 34, no. 10, pp. 7339–7349, Oct. 2023.

[22] Y. Shtessel, C. Edwards, L. Fridman, and A. Levant, *Sliding Mode Control and Observation*. New York, NY, USA: Birkhäuser, 2013.

[23] S. Katsura, "Advanced motion control based on quarry of environmental information," Ph.D. thesis, Dept. Syst. Des. Eng., Keio Univ., Tokyo, Japan, 2004.

[24] X. Yang, Y. Ge, W. Deng, and J. Yao, "Observer-based motion axis control for hydraulic actuation systems," *Chin. J. Aeronaut.*, vol. 36, no. 9, pp. 408–415, 2023.

**ŠEJLA DŽAKMIĆ** was born in Sarajevo, in 1992. She received the B.S. degree in electrical and electronics engineering and the M.S. degree in electrical engineering from the International University of Sarajevo, Bosnia and Herzegovina, in 2015 and 2017, respectively, where she is currently pursuing the Ph.D. degree in electrical engineering. From 2015 to 2018, she was an Assistant Researcher with the International University of Sarajevo, where she is a Senior Assistant. Her research interests include motion control systems, bilateral control, and real-world haptics.

**AMEL RAMDEDOVIĆ** received the B.S. degree in electrical and electronics engineering from the International University of Sarajevo, in 2023. His research interests include control system design, bilateral control, mechatronics, and machine learning.

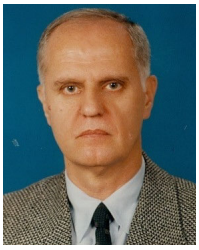

**ASIF ŠABANOVIĆ** (Life Senior Member, IEEE) received the B.S., M.S., and Dr.Eng. degrees in electrical engineering from the University of Sarajevo, Bosnia and Herzegovina. After graduation, he joined Energoinvest-IRCA Sarajevo. He was a Visiting Researcher with the IPU, Moscow; a Visiting Professor with Caltech, Pasadena, CA, USA; a Visiting Professor with Keio University, Yokohama, Japan; a Full Professor with Yamaguchi University, Ube, Japan; and the Head of the Department of Robotics, TÜBİTAK-MAM, Istanbul. He is currently an Emeritus Professor and a member of the Academy of Sciences and Arts of Bosnia and Herzegovina. His research interests include control systems, motion control systems, robotics, mechatronics, and power electronics.